Research Article

Affinity Maturated Transferrin Receptor Apical Domain Blocks Machupo Virus Glycoprotein Binding

Dick J. Sjöström [1], Birgit Grill [2], Elena Ambrosetti [3], Anuthariq Alikkam Veetil [1], Camilla Mohlin [1], Ana I. Teixeira [3], Gustav Oberdofer [2] and Sinisa Bjelic [1,*]

*1 - **Department of Chemistry and Biomedical Sciences,** Linnaeus University, Kalmar, Sweden*
*2 - **Department of Biochemistry,** Graz University of Technology, Graz, Austria*
*3 - **Department of Medical Biochemistry and Biophysics,** Karolinska Institutet, Sweden*

***Correspondence to Sinisa Bjelic:** Sinisa.Bjelic@lnu.se (S. Bjelic)*
https://doi.org/10.1016/j.jmb.2023.168262
Edited by Thomas J. Smith

Abstract

Transferrin receptor 1 (TfR) delivers iron across cellular membranes by shuttling the ion carrier protein transferrin. This ability to deliver large protein ligands inside cells is taken advantage of by pathogens to infiltrate human cells. Notably, the receptor's outermost ectodomain, the apical domain, is used as a point of attachment for several viruses including hemorrhagic arenaviruses. To better understand interactions with the receptor it would be advantageous to probe sequence determinants in the apical domain with viral spike proteins. Here, we carried out affinity maturation of our computationally designed apical domain from human TfR to identify underlying driving forces that lead to better binding. The improved variants were confirmed by in vitro surface plasmon resonance measurements with dissociation constants obtained in the lower nanomolar range. It was found that the strong binding affinities for the optimized variants matched the strength of interactions with the native receptor. The structure of the best variant was determined experimentally indicating that the conformational change in the hairpin binding motif at the protein–protein interface plays a crucial role. The experimental methodology can be straightforwardly applied to other arenavirus or pathogens that use the apical domain. It can further be useful to probe host–virus compatibility or therapeutic strategies based on the transferrin receptor decoys.

Introduction

Transferrin receptor 1 (TfR), expressed almost ubiquitously on the surface of human cells, is responsible for iron uptake across cellular membranes via the protein carrier transferrin[1]. Complex formation between the receptor and the ligand transferrin leads to internalization via endocytosis[2]. The functional form of the receptor forms obligatory dimers, where each subunit consists of three well-defined domains[3] and each domain is known for its specific interactions with both endogenous and exogenous proteins[4]. The helical domain is involved in transferrin binding forming the majority of contacts in the complex[5]. In addition, another endogenous regulatory protein, HFE, competes directly with the transferrin ligand for binding to the receptor helical domain[6–8]. Protease and apical domains have a less defined function for iron homeostasis, but the apical domain has been shown to be able to bind to the iron-carrier ferritin.[9] The primary function assigned to the apical domain, and partially to the protease domain, has been to form complexes with proteins expressed by pathogens, which via the receptor gain access to cells. Two well-characterized examples are viral glycoproteins

from New World *Arenaviridae* that solely use the apical domain of TfR for infection[10,11], while the malarial parasite targets the protease domain as well as the apical domain[12]. It has been recently suggested that the rabies virus glycoprotein also uses transferrin receptor interactions as an entry factor during endocytosis.[13]

Here, we investigate the interactions between apical domains and viral glycoproteins. Arenavirus-caused infections are present all over the world, including several diseases located in South America (Argentine, Bolivian, Venezuelan, and Brazilian haemorrhagic fevers) as well as Lassa fever in West Africa.[14] The agent pool is often maintained in rodents, re-emerging on a regular basis in rural, agricultural areas of developing countries. These are seasonal diseases that receive little or no attention but are in desperate need of novel therapies. The South American haemorrhagic fevers include one of the most studied diseases caused by the arenavirus with substantial outbreaks in Bolivia (Machupo virus). The spike protein present in these enveloped viruses is a homotrimer where each subunit is built from a signal peptide, glycoprotein 1, and glycoprotein 2. The signal peptide and the glycoproteins are associated into a heterotrimer after proteolytic cleavage of the glycoprotein precursor protein during viral maturation.[15] Glycoprotein 1 (GP1), the main mediator of binding to TfR, forms essential interactions required for cellular entry of both the Machupo and Junin variants.[10,11,16] Inhibiting complex formation between the viral glycoproteins and TfR apical domain offers inroads to preventing viral infections. Antibodies, as well as rodent-species standalone TfR apical domain (from White-throated woodrat, wwAP) have been demonstrated to have the potential to neutralize arenaviruses by binding directly to glycoprotein 1.[16,17] In addition, a circularly permutated, standalone apical domain can form a complex with a constant antibody domain (Fc) specifically modified in the CH3 region to achieve necessary binding interactions.[18]

We have recently engineered an apical domain variant (AP01) with the potential to be used as a decoy.[19] Using receptor decoys as neutralizing agents has shown potential, but their binding affinities to pathogens are usually lower than those of antibodies. Taking a receptor's domain out of its structural context often leads to a loss of avidity, or binding capacity in general, due to structural rearrangements. This has been observed in the case of TfR both for the wwAP[17] and for the decoupled apical domain from human TfR (AP01),[19] according to their respective experimentally determined structures. In both AP01 and wwAP, there occurs a restructuring of a long loop segment with a loss of crucial interactions. To use any receptors or their decoupled domain variants as antiviral agents, it is often necessary to improve binding through affinity maturation. To this end, we carried out directed evolution using the yeast surface display method combined with fluorescence-activated cell sorting (FACS). We further investigated whether the evolved AP01 towards the MGP1 target could lead to new insights into the molecular determinants of specific interactions between GP1 and human TfR. The methodology presented here has the potential to form a framework for investigating the evolutionary constraints guiding viral infections and for engineering potent therapeutic antivirals for medical applications against the Machupo virus or related strains.

Materials and Methods

Expression and purification of TfR and MGP1–Fc

Transferrin receptor was expressed and purified according to the protocol published in Sjöström et al.[20,21] MGP1–Fc (Fc portion of human IgG) in pHLsec plasmid was transfected into Expi293f cells, and was expressed and purified according to the published protocol.[17] Protein A agarose together with Protein A IgG Binding and Elution buffers (Pierce) were used for Fc–tagged MGP1 purification. The eluted proteins were purified by size exclusion chromatography (SEC) with Superdex 200 10/300 GL column (Cytiva) in HEPES buffer (20 mM HEPES, 100 mM NaCl, pH 7.6, and 10% glycerol).

AP01 A118E variant

AP01 gene in pETCON2 vector was according to the published work.[19] AP01 A118E forward and reverse primers, IDT (Integrated DNA Technologies), were used to introduce glutamate at position Ala^{118} by PCR amplification of the AP01–pETCON2 together with plasmid primers. The A118E mutant AP01 gene fragments and the linearized pETCON2 (*Xho* I/*Nde* I restriction sites) were transformed into *S. cerevisiae* yeast EBY100 strain. The transformants were selected on C–UT agar plates and confirmed by sequencing after colony PCR (Mix2Seq kit, EuroFins). Each colony was dissolved in zymolase solution (20 μL containing 5 mg/mL zymolase (Seikagaku corporation), 250 mM HEPES pH 7.4, 2 M sorbitol, and 15% glycerol) and incubated for 1 hour at 37 °C in the adaptation of protocol from Singh et al.[22] C–UT medium was prepared as in Chao et al.[23]: 1.85 g/L synthetic complete mixture, Kaiser, drop-out –*Trp* –*Ura* (Formedium), 6.9 g/L yeast nitrogen base without amino acids with ammonium sulfate (Formedium), and 20 g/L d-(+)-glucose (Sigma–Aldrich). For plasmid purification, cells were lysed with zymolase solution from 10 mL of yeast cells, grown ON to an OD_{600} = 6 in C–UT. QIAprep spin Miniprep Kit (Qiagen) was used to extract the plasmid.

Fluorescence-activated cell sorting of AP01 library

Plasmid pETCON2 containing AP01 A118E was the starting sequence for random mutagenesis (GeneMorph II, Agilent), where the sequencing primers were used to generate the library of AP01 A118E variants. Two reactions were set up with 3 and 300 ng AP01 A118E to determine the optimal number of mutations per gene. Both PCR reactions were transformed into yeast by electroporation in 0.2 cm cuvettes (Bio-Rad) at 2.5 kV, with 3 μg pETCON2, 9 μg AP01 A118E, conditioned with 0.1 M LiAc (Sigma–Aldrich), and 10 mM DTT (Fisher Bioreagents), in a volume of 400 μL following the published protocol.[24] The electroporated cells were transferred into 10 mL of a 1:1 mix of 2 M sorbitol and YPD medium (20 g/L peptone (Nordic Biolabs), 10 g/L yeast extract (Sigma-Aldrich), 20 g/L d-(+)-glucose (Sigma-Aldrich)), and incubated shaking at 30 °C for 1 hour. The cells were collected and resuspended in 50 mL C–UT medium, and the number of transformants was determined by plating 5 μL of the culture on selective C–UT agar plates.

Yeast surface display (YSD) method[23] was used to assay binding of AP01 A118E and variants thereof with target MGP1–Fc. During YSD both AP01 protein surface expression and binding to MGP1–Fc were determined by quantifying the increase of respective fluorescence signal by bound protein conjugates. In brief, EBY100 yeast cells were passaged overnight in C–UT medium to OD_{600} of 5–6. The protein surface expression was induced by switching to C–UT medium containing galactose instead of glucose with a final OD_{600} = 0.75, incubated at 20 °C shaking at 200 rpm for 24 hours. 1.5 mL (approximately 3×10^7) induced cells were washed with 3 mL PBSF (8g NaCl, 0.2 g KCl, 1.44 g Na_2HPO_4, 0.24 g KH_2PO_4 and 1 g bovine serum albumin in 1 L deionized sterile filtered H_2O, adjusted to pH 7.4). Cells were labelled on ice for 1.5 hours initially at 3 μM MGP1–Fc (or lower at 30 nM for S3 sorting round), filled up to 1.5 mL with PBSF. With samples kept on ice until measurement, another wash with 3 mL PBSF was performed before 30 minutes of labelling with 1:100 of diluted Chicken anti-c-Myc FITC conjugated antibody that monitored yeast surface protein expression (Immunology Consultants Laboratory) and 1:100 Rhodamine (TRITC) Affini-Pure Goat Anti-Human IgG, Fcγ fragment specific (Jackson IR) that detected MGP1–Fc binding to yeast expressed protein, reaching a total volume of 1.5 mL with PBSF. The cells were washed with PBSF and after resuspension in PBSF sorted with a BioRad S3e instrument. Both FITC and TRITC were excited with a 488 nm blue laser. The band-pass filters used to detect FITC and TRITC were 525/30 and 586/25. Crossover fluorescence was compensated with single-stained samples with 15 μM MGP1–Fc. Cells were gated on the top 1% during rounds of fluorescence-activated cell sorting (FACS) in a triangular gate on the diagonal top left of the FITC/TRITC positive population. Cells were collected in C–UT supplemented with penicillin and streptomycin. Between each round of FACS, the cells were passaged twice in 50 mL C–UT medium.

Yeast surface displayed AP01 or its variants, were assayed for binding to MGP1–Fc by flow cytometry (FC) on BD Accuri C6. Protein expression on yeast cells was carried out as described above for FACS sorting of the AP01 library. Labelling was according to above but in 30 μL volume (approximately 4×10^5 cells).

In vitro binding assay

AP01 variants were cloned into pET29b(+) vector, expressed, and purified by immobilized metal ion affinity chromatography (IMAC) followed by SEC according to Sjöström et al.[19] Biacore T200 instrument (Cytiva) was used to perform surface plasmon resonance (SPR) measurement experiments. MGP1–Fc [17] proteins were immobilized on Protein A sensorchip (Cytiva) by injecting them over the surface at 20 μg/mL with a flow rate of 20 μL/min in HBS-P+ (HEPES 10 mM, NaCl 150 mM, p20 0.05%) running buffer (Cytiva) until reaching an immobilization level of 3000 RU. The binding affinity of AP01, the variants S2.2, S2.3, S3.3, S3.4, S3.6, and TfR[20] was preliminarily evaluated by injecting each protein at a single concentration of 2 μM in the running buffer. The preliminary estimation of the K_d was used to select the concentrations to be tested in the kinetic analysis. The protein concentrations tested were 0.05, 0.14, 0.4, 1.2, and 3.7 μM for AP01; 3.7, 11.1, 33.3, 100, and 300 nM for S2.2, S2.3 S.3.3, S3.4 and S.3.6; 10.6, 31.9, 95.6, 286.7, and 860 nM for TfR. Each sample was injected using a single cycle kinetic mode with an association phase of 150 s and a dissociation phase of 4000 s, needed for complete dissociation of the proteins from the surface. The kinetic parameters were determined using the BIAEVALUATION 3.0 software, assuming a 1:1 binding model.

HeLa cell-based assay

The human epithelial HeLa cell line was cultured in Dulbecco´s modified Eagle´s medium (DMEM) without phenol red (Gibco) supplemented with 10% fetal bovine serum, Glutamax (Invitrogen), penicillin, and 100 μg/mL streptomycin at 37 °C under a humified 5% CO_2 atmosphere and subcultured when confluent (chemicals from Sigma–Aldrich). HeLa cells were seeded on six-well plates, 2×10^5 cells/well, and allowed to grow for 48 h. MGP1–Fc at 10 nM was allowed to interact with 1:100 dilution of F(ab')2-goat anti-human IgG Fc secondary antibody, PE conjugate (Invitrogen), and AP01 S2.3 variant at three

different concentrations, 0.01 μM, 0.1 μM, and 1 μM, in a cell culture medium for 25 minutes, in the dark. Confluent HeLa cells were washed twice in PBS and thereafter exposed to MGP1–Fc/anti-Fc–PE only or MGP1–Fc/anti-Fc–PE incubated together with S2.3 for 2 hours at 37 °C under a humified 5% CO_2 atmosphere. Cells in anti-Fc–PE (1:100 dilution) alone served as a negative control. Plates were rotated three times during the incubation. Cells were scraped, washed in PBS, and strained for the flow cytometry assay.

HeLa cells were mounted with anti-fading mounting medium Vectashield containing 4′,6-dia midino-2-phenylindole (DAPI), Vector Laboratories (Burlingame). Images were captured with an epifluorescence microscope (Nikon) using the software Nis-element imaging, version 4.3 (Nikon), or by using a confocal microscope (Nikon) and the confocal microscope EZ-C1 2.20 software. Pictures were bright-adjusted in Adobe Photoshop version 23.5.4.

Experimental structure determination of AP01 S2.3

BL21 (DE3) STAR *E. coli* strain (ThermoFisher Scientific) was used for protein expression. The overnight culture was diluted 1:100 in TB media and grown at 37 °C and 180 rpm. When the optical density OD_{600} reached 0.7, the temperature was lowered to 25 °C, and the protein was induced by 0.1 mM IPTG for 20 hours. Cells were harvested at 4,500 × *g* for 15 min and washed with 0.9 % NaCl. Each gram of cell pellet was dissolved in 10 mL 20 mM NaPi, 500 mM NaCl, 20 mM imidazole, pH 7.4, and sonicated on ice for 15 min at 70 % duty cycle and 50 W using a Labsonic U (Braun) sonicator. Lysed cells were centrifuged at 39,000 × *g* for 45 min. The supernatant was filtered through a 0.45 μm filter and loaded on a 5 mL HisTrap HP column (GE Healthcare), pre-equilibrated with 20 mM NaPi, 500 mM NaCl, 20 mM imidazole, pH 7.4. The column was washed with 20 mM NaPi, 500 mM NaCl, 30 mM imidazole, pH 7.4, followed by 20 mM NaPi, 1000 mM NaCl, 30 mM imidazole, pH 7.4, followed by 20 mM NaPi, 500 mM NaCl, 60 mM imidazole, pH 7.4, and eluted with 20 mM NaPi, 500 mM NaCl, 250 mM imidazole, pH 7.4. Elutes, containing the protein of the correct size, were confirmed with SDSPAGE, concentrated, and further purified by SEC over Superdex 75 Increase 10/300 GL column using a buffer containing 20 mM HEPES, pH 6.8, 150 mM NaCl, 1 mM TCEP. The cleanest fractions, as determined by SDS–PAGE, were pooled and concentrated to 13 mg/mL (OD280) for crystallization setups.

Crystallization drops were set up with commercial crystallization screens using the vapor diffusion method employing a mosquito® Xtal3 crystallization robot (SPT Labtech) and incubated at 293 K. The drop volume was 270 nL, with different ratios of protein and precipitant solution (1:1, 1:2, and 2:1). Clusters of rod-shaped crystals appeared after three days in 100 mM MIB, pH 7, and 25 % PEG 1500 (Molecular Dimension PACT premier screen, condition 16). Optimization setups, using the vapor diffusion method resulted in diffraction quality crystals grown by mixing 0.5 μL of 11 mg/mL protein in 20 mM HEPES, pH 6.8, 150 mM NaCl with 1 μL of 100 mM MIB buffer, pH 7.5, and 24 % PEG. The obtained crystals were harvested from mother liquor with CryoLoops (Hampton Research) and briefly incubated with mother liquor containing 25% glycerol, followed by flash freezing in liquid nitrogen. Diffraction data was collected at 100 K on beamline P11 at DESY (Hamburg, Germany). A full dataset (360°) was collected to 1.8 Å resolution from a monoclinic crystal (space group $P12_11$).

The collected data were processed using XDS[25,26] with the provided input file from the beamline. Structure determination was performed by molecular replacement using PHASER [27] with the structure of AP01 (PDB ID 6y76) as a search template. The best solution was refined in reciprocal space with PHENIX,[28] with 5% of the data used for R_{free} and by real-space fitting steps against σA-weighted *2Fo–Fc* and *Fo–Fc* electron density maps using COOT. Water molecules were placed automatically into difference electron maps and accepted or rejected according to geometry criteria and their B-factors, defined in the refinement protocol. The final model could be refined to $R = 21.34\%$

Figure 1. AP01 A118E variant interacts stronger with MGP1 than the native AP01 according to flow cytometry measurements of yeast displayed variants. (A) The redesigned loop in the AP01 structure adopts a different conformation in comparison when hTfR apical domain is in the complex with MGP1, leading to the corresponding glutamate 294 of TfR (AP01 glutamate 99) positioned away in the modelled interface. (B) The salt bridge formed between E294 and K169 in the apical domain of TfR and MGP1, respectively (PDB ID 3kas and numbering). (C) A modelled complex of AP01 (PDB ID 6y76) superimposed on the apical domain of the transferrin receptor. A salt-bridge interaction was recovered by introducing glutamate at position A118. Flow cytometry measurements of MGP1–Fc binding to AP01 (D) or AP01 A118E (E) displayed on the yeast surface. The mutant shows a clear increase in the binding signal (top panel) compared to the background signal (lower panel). Variants were assayed at 15 μM MGP1–Fc concentration.

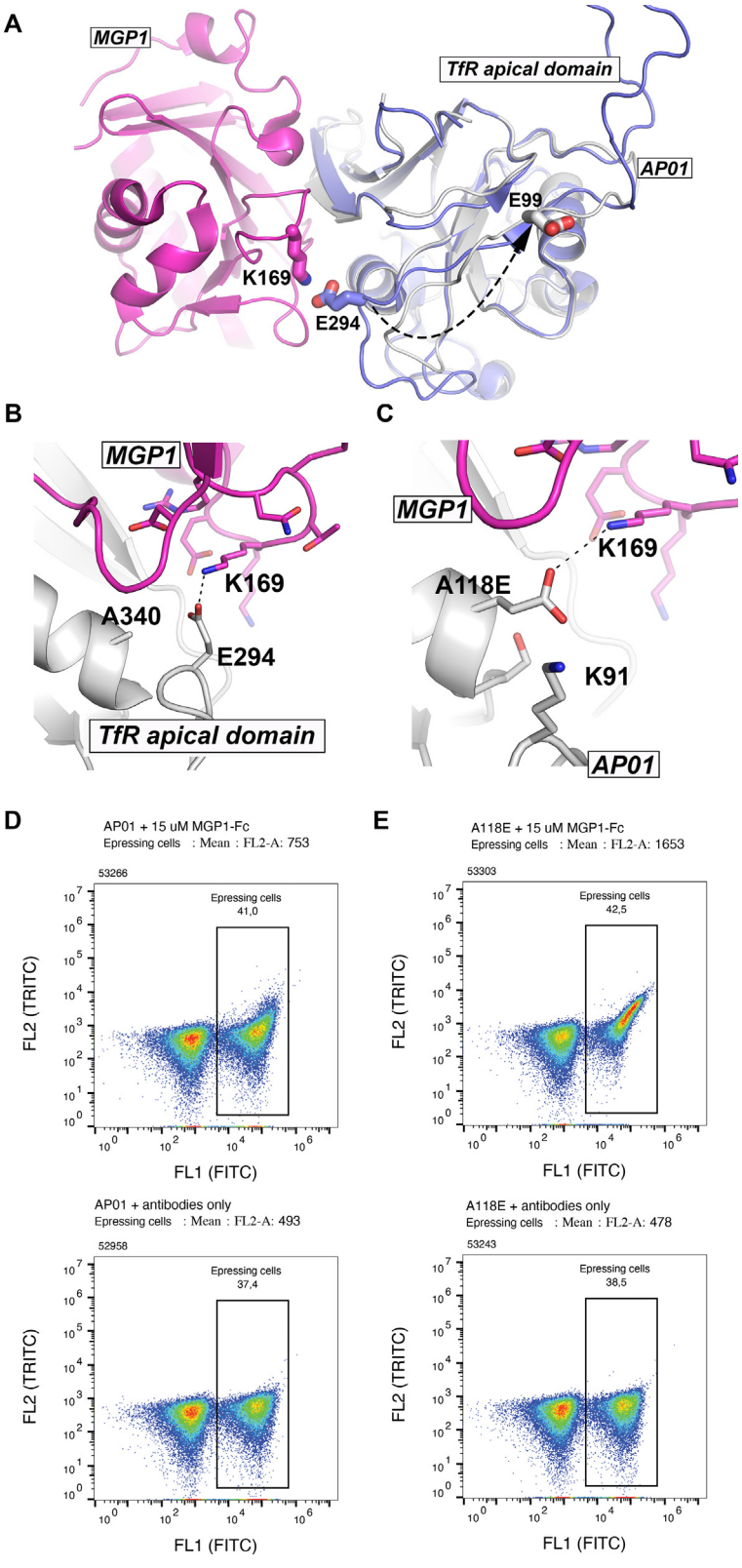
A
MGP1
TfR apical domain
AP01
E99
K169
E294
B
MGP1
K169
A340
E294
TfR apical domain
C
MGP1
K169
A118E
K91
AP01
D
AP01 + 15 uM MGP1-Fc
Epressing cells : Mean : FL2-A: 753
53266
Epressing cells
41,0
FL2 (TRITC)
FL1 (FITC)
AP01 + antibodies only
Epressing cells : Mean : FL2-A: 493
52958
Epressing cells
37,4
FL2 (TRITC)
FL1 (FITC)
E
A118E + 15 uM MGP1-Fc
Epressing cells : Mean : FL2-A: 1653
53303
Epressing cells
42,5
FL2 (TRITC)
FL1 (FITC)
A118E + antibodies only
Epressing cells : Mean : FL2-A: 478
53243
Epressing cells
38,5
FL2 (TRITC)
FL1 (FITC)

and R_{free} = 23.63%. No electron density was observed for the last 11 residues. Details of data collection, processing, and refinement are summarized in Table S1.

Results

Validation of AP01 A118E binding to MGP1–Fc

Visual inspection of TfR in complex with MGP1 (PDB ID 3kas) and the corresponding apo structure of the standalone apical domain (PDB ID 6y76) indicated that there was a loss of a salt bridge interaction present in the native complex. Due to the design process in which several interface residues between the apical and the protease domains of TfR had been mutated to hydrophilic residues, in addition to the deletion of a long unstructured region protruding out of the apical domain, a rearrangement occurred in the redesigned loop of AP01 (Figure 1(A) and Figure 5 in Sjöström et al.).[19] Whereas in the complex formed between TfR and MGP1, glutamate at position 294 is at a hydrogen-bonding distance from Lys^{169} (Figure 1(B)), in the AP01 structure the loop carrying the corresponding glutamate was in a conformation unproductive for binding (Figure 1(A)). The salt bridge interaction was reintroduced by mutating the alanine residue at position 118 (Ala^{340} in TfR) to glutamate, situated on the adjacent alpha helix in AP01 relative to the rearranged loop (Figure 1(C)).

To measure the relative binding interaction between MGP1 and native AP01 in comparison to the A118E variant, the two proteins were displayed on the yeast surface, and MGP1 binding was measured by flow cytometry. MGP1–Fc, with the corresponding increase in the binding signal upon interaction with the displayed protein, was detected by emission from anti-Fc Ab coupled to tetramethylrhodamine (TRITC). The level of expressing cells was similarly measured by anti-c-Myc Ab coupled to FITC where the c-Myc tag was co-expressed with the displayed protein. From the measurements, we observed an apparent increase in the binding signal for the expressing population (Figure 1(D,E) top panel) in comparison to the background signal (Figure 1(D, E) lower panel). The AP01 A118E variant had approximately 5 times stronger signal over the background compared to the native AP01 protein, assayed at 15 μM MGP1–Fc concentration. The A118E mutation allowed us to sort and select better binding variants at a lower concentration of MGP1–Fc.

AP01 A118E optimization by FACS

Titration of yeast displayed AP01 A118E with MGP1–Fc was measured by flow cytometry to determine a suitable concentration range for binding optimization. The titrated K_d for the interaction was determined to 3.0 μM (Figure S1), which was chosen as the initial concentration for selection by FACS. The initial library, S0, generated by error-prone mutagenesis, was approximately 4×10^6 variants before sorting at 3 μM MGP1–Fc. The subsequent sorting of S1 was at the same concentration of MGP1–Fc while for S2 it was lowered to 30 nM target. About 10 colonies were picked randomly for sequencing to inquire about the library variability at each sorting round (Table S2). Retesting S0–S2 at 300 nM MGP1 indicated a clear increase in the binding signal when assayed by YSD/FC (Figure 2 top panels). Sort 1 retained a random population as expected after the initial sorting of the naïve library. In contrast, S2 converged to V15 mutation. We tested individually three variants from S2 for MGP1–Fc binding: flow cytometry data showed a clear binding signal at 300 nM (Figure 2 lower panels, Table 1). Additional sorting and sequencing did not indicate any significantly different variants from Sort 3 (Table S2).

SPR measurement of evolved AP01 variants with MGP1–Fc

To confirm the increase in binding strength between MGP1 and the evolved variants from the YSD selection experiments, we carried out surface plasmon resonance (SPR) measurements in single cycle kinetic mode. Protein A coated SPR sensor chips were used to immobilize target MGP1–Fc proteins. We measured the binding affinity of AP01 and five evolved variants (Table 1), bacterially expressed and purified by IMAC/SEC, and determined their dissociation constants (K_d) (Table 2, Figure 3). TfR was used as the positive control for binding interaction to the immobilized MGP1–Fc. The initially designed AP01 construct bound to MGP1–Fc in the micromolar range (K_d = 3 μM,) indicating about 400 times loss in binding affinity compared to native TfR (K_d = 8.2 nM) (Table 2). This can be partially explained due to the loss of avidity effects, as TfR is dimeric, but also partially due to the loss of the ion pair interaction (Figure 1(A,B)). From the YSD/FC measurements we observed that the introduction of the A118E mutation, which recovers the lost charge–charge interaction during complex formation, increases the binding affinity about five times.

The evolved variants chosen for SPR testing were based on the predominance of the V15E mutation. Additionally, mutation to V15A was also validated. Besides these mutations, the remaining variants contained changes distributed throughout the sequence. From the SPR measurements, the highest binding affinities were observed for the S2.3 and S3.4 mutants, with dissociation constants of 15 nM and 17 nM, respectively, which are approximately 240 times stronger than for the native AP01. This evidence suggested that

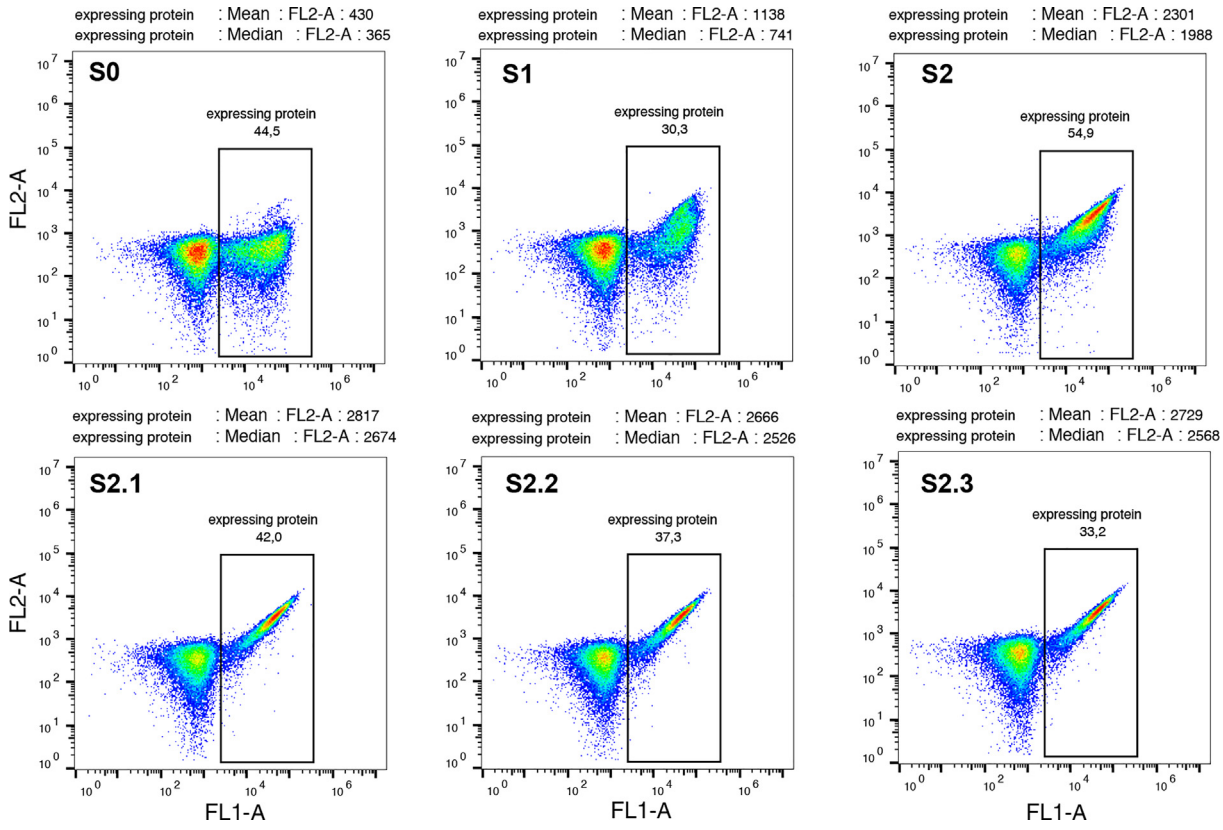

Figure 2. Validation of sorts S0–S2 and S2 variants: S2.1, S2.2, S2.3 at 300 nM concentration MGP1–Fc. There is a clear increase in the binding signal for the expressing cells during the sorting rounds. Variants found in S2 (S2.1–S2.3) bind strongly to the target glycoprotein at the tested concentration.

Table 1 AP01 variants validated by YSD/FC or SPR.

Variant	Mutations	YSD/FC	SPR K_d (nM)
AP01	native	Low signal	×
AP01 *variant*	**A118E**	×	–
S2.1	V15E/**A118E**/S133G	×	–
S2.2	V15E/**A118E**/G157D	×	×
S2.3	V15E/**A118E**/S156G/S158R	×	×
S3.3	V15A/**A118E**	–	×
S3.4	V15E/**A118E**	–	×
S3.6	V15E/Y52H/G65D/ Q90R/ **A118E**	–	×

Table 2 SPR measurements of MGP1–Fc interaction with TfR, AP01, or S2/S3 variants.

Variant	k_{on} [1/(Ms)]	k_{off} [1/s]	K_d [nM]
AP01	3500	0.013	3 600
S2.2	6.6E+04	0.0013	20
S2.3	8.8E+04	0.0013	15
S3.3	7.7E+04	0.0042	55
S3.4	1.2E+05	0.0020	17
S3.6	2.7E+05	0.016	57
TfR	8700	7.1E–05	8.2[a]

[a] Apparent dissociation constant due to the avidity of the dimeric TfR.

the largest gain in binding affinity was obtained with the V15E mutation. These variants also reduced the gap lost upon the redesign of the TfR apical domain, resulting in dissociation constants that approach the value exhibited by TfR (K_d = 8.2 nM). On the contrary, the S3.3 variant, which contains V15A mutation allowing for direct comparison with S3.4, resulted in a slightly weaker complex formation (K_d = 55 nM). The S3.6 variant had V15E mutation in addition to other changes that resulted in slightly higher K_d than for the other V15E-containing variants.

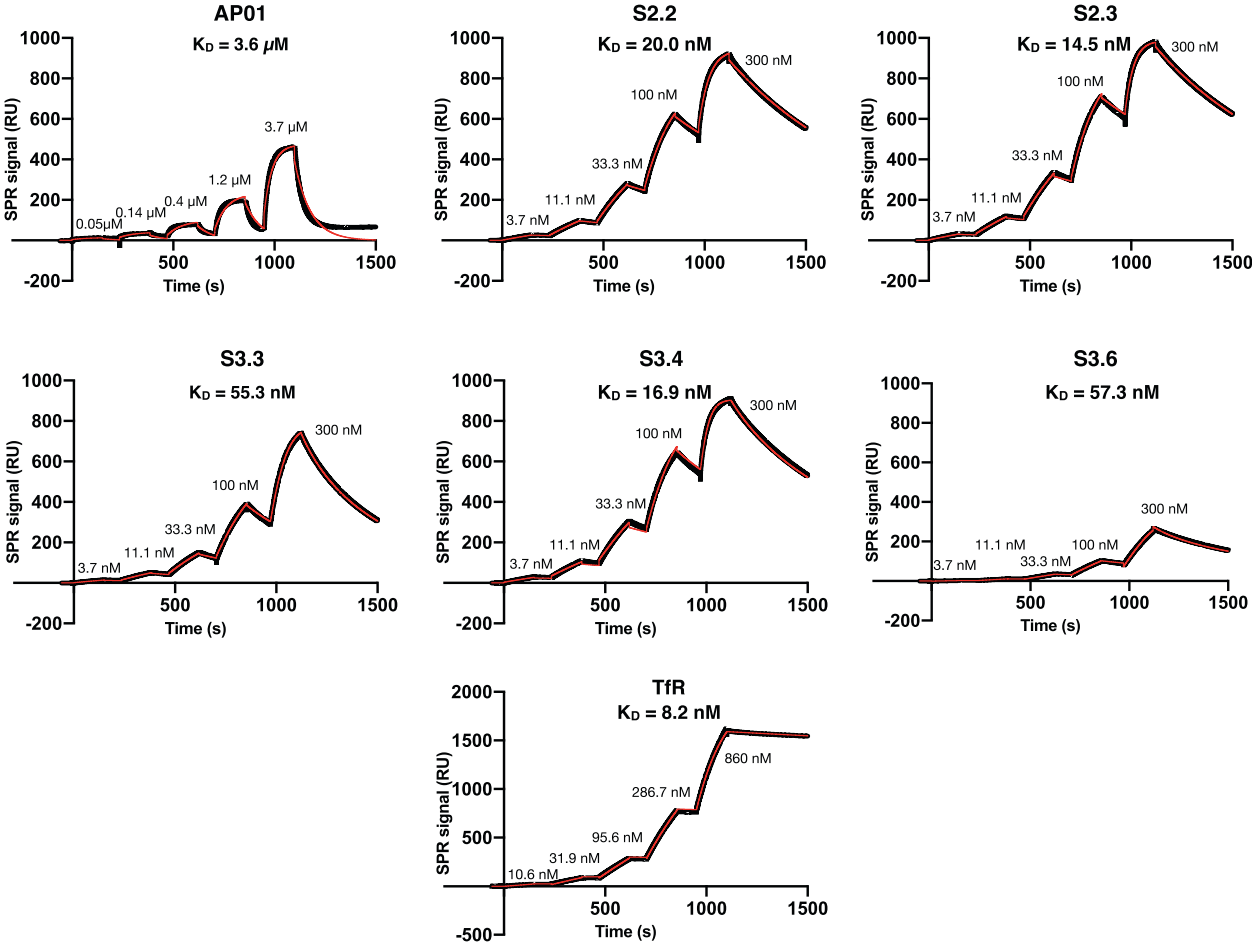

Figure 3. Surface plasmon resonance measurements of AP01 and its variants with MGP1–Fc immobilized on the protein A sensor chip. Single cycle kinetics were carried out to determine the dissociation rate constants. AP01, the redesigned apical domain of TfR, showed low micromolar interaction with the Machupo glycoprotein 1, while the evolved variants were in the lower nanomolar range. Transferrin receptor, TfR, binding to MGP1 was also determined (apparent dissociation constant) to K_d = 8.2 nM as a control and a reference. The experiment was repeated twice with lower immobilization of MGP1 without any significant differences for the calculated dissociation constants. The red line is the calculated fit to the obtained measurement in black.

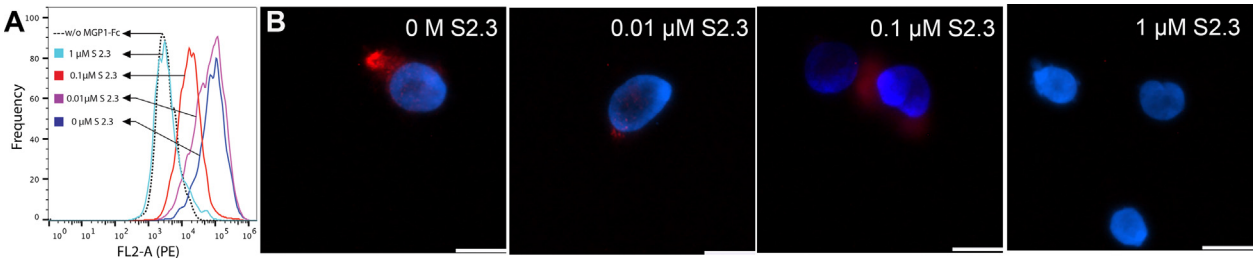

Figure 4. AP01–S2.3 variant competes with MGP1 for TfR binding. (A) Flow cytometry assay of HeLa cells assayed with 10 nM MGP1–Fc labelled with anti-Fc PE and different concentrations of S2.3. The binding signal is diminished at increasing concentrations of S2.3 to be completely lost by the addition of 1 μM S2.3 (the signal overlaps for cells w/o MGP1–Fc added). (B) Representative fluorescent images of HeLa cells from flow cytometry assay. The fluorescent signal of bound MGP1 (at 0 M S2.3) decreases in the presence of higher concentrations of S2.3 following the dose-dependent behavior. The bar indicates 10 μm.

S2.3 evolved variant blocks MGP1 uptake

The evolved AP01 variants were additionally validated in a cell-based assay. For this purpose, HeLa cells, known to overexpress TfR, were assayed for MGP1 binding alone and in competition with AP01 S2.3 variant by both flow cytometry and microscopy (Figure 4). In the assays, the cells were treated with 10 nM MGP1–Fc and the binding was measured by detection of anti-Fc Ab PE. A clear shift in the signal assayed by flow cytometry was observed for the MGP1 binding relative to the negative control, which was DAPI-stained cells without any MGP1 added (Figure 4(A)). Adding the S2.3 variant at increasing concentrations led to a clear shift in the binding signal towards the negative control. The concentration of S2.3 at 1 μM resulted in a total loss of the binding signal, and a tenfold lower concentration gave about 50% of the signal. The cells showed the corresponding trend when inspected visually in the microscope (Figure 4(B)). Overall, the addition of S2.3 decreased the binding signal in a dose-dependent manner validating its ability to block MGP1 binding to human cells and consequently the uptake.

Experimental structure of S2.3

The most frequent variant during selection carried V15E mutation which also contributed most strongly to complex formation according to the measured K_d values. The Val^{15} residue is situated in the binding motif that also carries the known hotspot residue Tyr^{211} in TfR (equivalent to Tyr^{16} in AP01). In the MGP1–TfR complex (PDB ID 3kas) this valine side chain is on the opposite face of the beta-strand in comparison to Tyr^{211} (Figure 5(A)). On

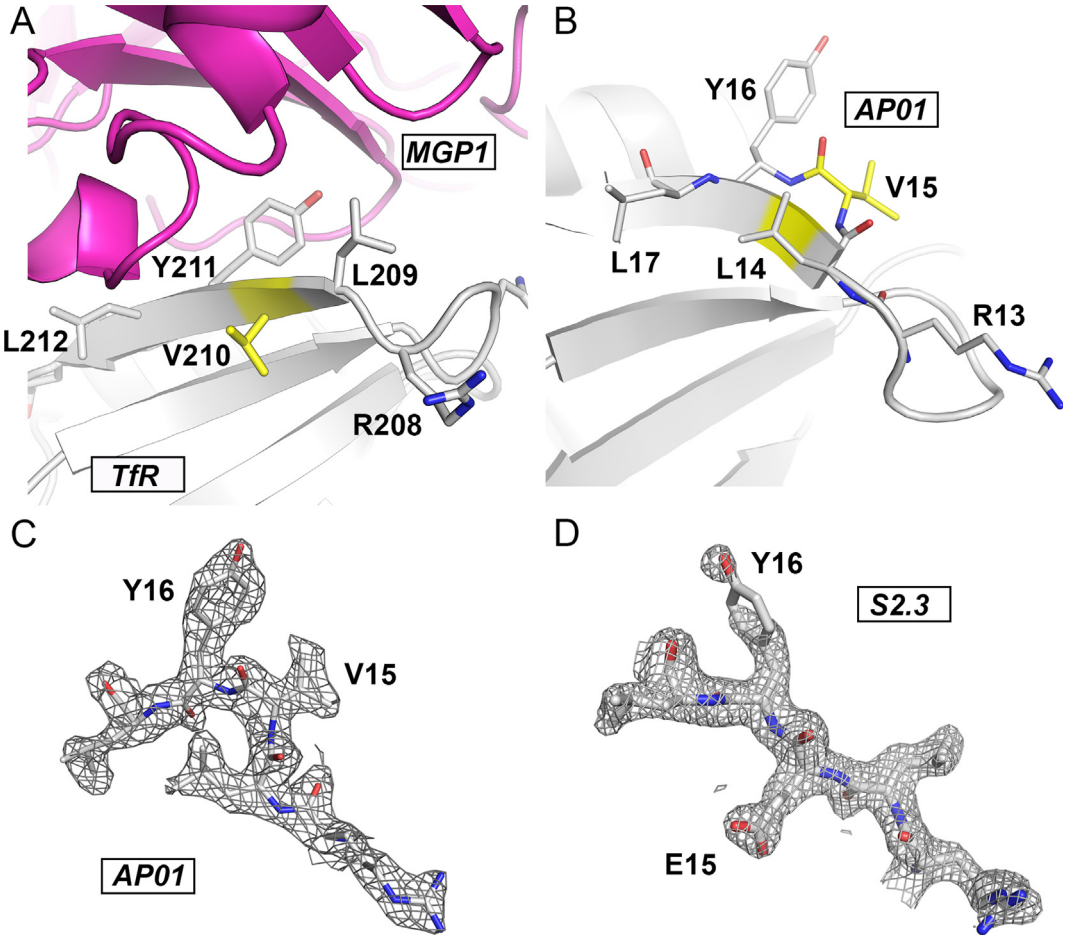

Figure 5. The evolved mutation, V15E, may stabilize the apical domain as well as AP01 in a conformation that is more productive for binding MGP1. (A) MGP1 in complex with TfR (PDB ID 3kas) with the side chain of valine at position 210 (yellow) pointing to the opposite side of the beta-strand in comparison to tyrosine at 211. (B) In the apo AP01 structure (PDB ID 6y76), the corresponding side chain of valine (position 15 in the apical domain in yellow) pointed along the same direction as the tyrosine side chain. (C) Density around the valine, V15, and the tyrosine, Y16, were clearly resolved. (D) Density for the binding motif with the E15 side chain facing the opposite direction compared to the V15 in AP01. The V15E mutation stabilizes the binding motif in a conformation that is substantially more productive for binding as it resembles the complexed orientation.

the contrary, in the Apo AP01 structure (PDB ID 6y76), the corresponding valine (Val^{15}) is on the same side of the beta-strand as the hotspot tyrosine (Figure 5(B)) which is also confirmed by the 2*Fo-Fc* density map (Figure 5(C)). The V15E mutation would therefore place the negatively charged glutamate side chain at an energetically unfavorable orientation with respect to the tyrosine (close to π-orbitals of the tyrosine aromatic ring). We speculated that this leads to the glutamate residue rearranging at the opposite face of the strand in comparison to the Tyr^{211} resulting in a motif conformation that is substantially more productive for binding. To test the hypothesis that the apo structure of S2.3 should have the E15 side chain pointing in the opposite direction compared to AP01 native variant we solved the experimental structure of S2.3. The 2*Fo-Fc* density map for the binding motif showed well-resolved side chains but for the hotspot tyrosine at position 16 (Figure 5(D)). The glutamate mutation at the adjacent position 15 confirmed the side chain with the carboxyl group facing in the opposite direction of the tyrosine, towards Lys^{152}. However, the ion pair interaction was not fully formed at the 5.3 Å distance between Glu^{15} and Lys^{152} in the solved structure. The leucine side chain at position 14 also switches the direction due to the conformational changes in the motif, aligning in the same direction as the Tyr^{16}. We conclude that the evolved mutation V15E in the binding motif stabilizes the conformation for optimal interaction with MGP1.

Discussion

We demonstrate that we can evolve our previously designed, decoupled TfR apical domain, AP01, from a micromolar dissociation constant with MGP1 to low nanomolar binding, with a K_d of ~15 nM. The affinity of the S2.3 variant of AP01 to MGP1 was almost on parity with that of the full receptor ectodomain, taking into account the avidity of the dimeric form of TfR, with an apparent dissociation constant of 8 nM. The reported value for MGP1–Fc binding to hTfR was $K_d^{apparent}$ = 27 nM as determined by SPR measurements,[29] thus in agreement with our values. Similarly, the published dissociation constants for endogenous ligands transferrin and HFE binding to hTfR are 1 nM and 24–89 nM, respectively.[6,7] Further, we showed that the best variant, S2.3, efficiently blocked MGP1 uptake in HeLa cell-based assays. A single HeLa cell expresses approximately 10^5 TfR molecules on its surface[30] and Hela cells have been used previously as a model system to demonstrate the uptake of viruses pseudotyped with Machupo glycoprotein precursor.[11,31] The mutations in the evolved variants, including S2.3, were predominantly situated in the beta-hairpin structural motif, encompassing residues 208–212 in hTfR, which was shown to be essential for binding to MGP1[10,32] and found to be under the selective pressure in arenaviral hosts species i.e., rodents (residues 205, 209 and 215 hTfR numbering). The most favorable mutation during YSD/FACS selection was observed at position 15 in AP01, where the change into glutamate at that position, V15E, together with the previously introduced mutation A118E resulted in a 17 nM dissociation binding constant. Position 15 is on one of the strands in the beta-hairpin motif, thus adjacent to the hotspot residue Tyr^{16} (in TfR Tyr^{211}).[32] Moreover, the mutation to alanine, V15A, together with A118E, resulted in a three times poorer dissociation constant with respect to the V15E/A118E.

Structural data suggests that the glutamate side chain at position 15 in the evolved variants of the apical domain might influence the conformation of the hairpin motif towards a state more productive for binding. For example, Val^{210} in the solved complex of MGP1–TfR (PDB ID 3kas[10]) had the side chain in the opposite orientation when compared to Val^{15} in the apo structure of AP01 (Figure S2(A)). Since the side chain at position 15 would clash with MGP1 upon binding, it has to either rotate out of the way before the complex is formed or, alternatively, this conformation has to be already preformed in the apo state. To investigate this, we determined the experimental structure of S2.3, which resolved the glutamate side chain as hypothesized in the complex-favoring orientation (Figure S2(B)). Interestingly, when compared to the standalone apical domain from White-throated woodrat (wwAP), which also has low nanomolar binding to MGP1 with K_d = 4 nM, the binding motif had a leucine (at the corresponding position of AP01 Val^{15}) facing as well away from the complexed MGP1 (PDB ID 6s9j,[17] Figure S2 and Figure S3). Furthermore, in Figure S2(B), the leucine 209 side chain of wwAP is at 3.4 Å from the amine group of Lys^{374} (corresponding valine–lysine in 3kas is at 4.9 Å; Glu^{15} is at 5.9 Å from the lysine 152 in AP01). Although the distance in S2.3 is beyond optimal for charge–charge interaction, in the complex the residues may come closer to favor the productive conformation of the binding motif. From published alignments data for TfR orthologs (Figure 3 in Radoshitzky et al.[32] and Figure 2 in Kerr et al.[33]), the residue variability at the position prior to Tyr^{211} was leucine, valine, alanine, serine, or isoleucine. These alignments include host species TfR specific for respective arenavirus and are best interpreted in their respective structural context. They do, however, indicate the possible variability at that position. In comparison, from the alignments, it can be inferred that the hotspot residue Tyr^{211} was largely conserved (only aspartate additionally observed); the similar was observed for the residue Leu^{212} where instead a proline occurred. Additionally, tyrosine 211 mutation to threonine was shown to block MGP1 binding to hTfR.[32] From the published muta-

genesis data L212V mutation in hTfR protects partially against the Machupo arenavirus infection[34] (the Val^{212} mutant was not found in relation to arenaviruses).

It would be of interest to determine the interactions necessary for higher affinity binding to the other arenaviruses known to infect humans. The binding of wwAP to viral glycoproteins had, for example, K_d values 4 nM and 1 μM for interaction with MACV and JUNV, respectively[17]. Additional work by Kerr et el.[33] evaluated the binding predictions of MGP1 to different variants of TfR with the goal of determining host–virus compatibility. The predictions were generally consistent, however, attempts to evaluate interactions with other virus strains were unsuccessful due to the lack of experimental structures. While determining the structure of each complex is cumbersome, the observed conformational changes with the induced fit-like binding events are in general challenging to predict and require additional data from experiments to be reliable. Interestingly, designed proteins that target the apical domain as in the MGP1–TfR complex conformation (PDB id 3kas[10] were unproductive).[35] More success was obtained towards the apical domain conformation found in the designed protein bound to hTfR (PDB id 6wrx).[35] An alternative conformation of the beta-hairpin motif exists in the latter complex, including the hotspot residue, that appeared more productive for protein design applications. Finally, the structure of the circularly permutated apical domain bound to the engineered Fc-domain[18] revealed the conformation of the apical domain binding motif conforming to the one in the AP01 structure (Figure S4). In the Fc–apical domain complex the tyrosine side chain and the beta-hairpin motif are not directly involved in binding as with MGP1.

To improve possible therapeutic properties of receptor decoys, it is often advantageous to couple them to the Fc region of antibodies. In addition to mediating Fc-effector functions, which have been proven crucial for the therapeutic efficacy of clinically relevant antibodies, the resulting configuration of the fused protein should gain in binding strength due to the avidity of the dimerizing Fc part. The Fc-fused construct had been successfully validated for the wwAP receptor decoy and this strategy could be applied as well on the evolved variants of AP01. It would be interesting to test whether such constructs of the AP01 S2.3 variant could lead to any gain in potency. Specifically, when compared to antibodies that have been developed against hemorrhagic fevers, an additional improvement in affinity needs to be realized to achieve any significant therapeutic impact. Junin virus elicited antibodies, that bind specifically to the GP1 receptor binding surface, had K_d values reported at 45 pM, 5 nM, and 86 nM.[36] The same antibodies had the strongest affinity of K_d = 16 nM for MGP1. For any future therapeutic applications, another round of directed evolution would be beneficial to achieve tighter binding besides exploring Fc-fusion variants.

In summary, the methodology outlined here, with a combination of affinity maturation experiments carried out on the apical domain of TfR with computational design to facilitate solubilization of the receptor domain, allows for better assessment of different arenavirus compatibility towards human TfR. In our previous work, we demonstrated that selection experiments can be carried out also on the viral glycoproteins,[20] opening up the possibility to test host–virus compatibility in an in-lab evolutionary setting. We propose that the combination of experiments, protein–protein interface residue scanning,[37] and protein backbone design[19] presented here may be explored to improve engineered binding apical domain variants towards other South American hemorrhagic fevers.

Accession Number

Coordinates and structure factors have been deposited in the Protein Data Bank with accession number 8p0z.

CRediT authorship contribution statement

Dick J. Sjöström: Investigation, Writing – review & editing. **Birgit Grill:** Investigation, Writing – review & editing. **Elena Ambrosetti:** Investigation, Writing – review & editing. **Anuthariq Alikkam Veetil:** Investigation, Writing – review & editing. **Camilla Mohlin:** Resources, Methodology, Writing – review & editing. **Ana I. Teixeira:** Resources, Methodology, Writing – review & editing. **Gustav Oberdofer:** Resources, Methodology, Writing – review & editing. **Sinisa Bjelic:** Resources, Conceptualization, Supervision, Investigation, Methodology, Writing – original draft.

DATA AVAILABILITY

Data will be made available on request.

DECLARATION OF COMPETING INTEREST

The authors declare that they have no known competing financial interests or personal relationships that could have appeared to influence the work reported in this paper.

Acknowledgments

MGP1–Fc in pHLsec vector was generously shared by Ron Diskin's lab, Weizmann Institute

of Science. SB is grateful for financial support from The Crafoord Foundation (20200765). BG and GO are supported by the ERC-Starting Grant HelixMold (802217) and by the Austrian Science Fund (FWF) project P30826. We are thankful for TfR expression and purification carried out by Juni Andréll, Science for Life Laboratories.

Appendix A. Supplementary Data

Supplementary data to this article can be found online at https://doi.org/10.1016/j.jmb.2023.168262.

Received 3 July 2023;
Accepted 29 August 2023;
Available online 9 September 2023

Keywords:
transferrin receptor;
yeast surface display;
Rosetta;
protein design

Abbreviations:
FC, fllow cytometry; Tf, Transferrin; TfR, transferrin receptor 1; YSD, yeast surface display

References

1. Andrews, N.C., Schmidt, P.J., (2007). Iron homeostasis. *Annu. Rev. Physiol.* **69**, 69–85.
2. Eckenroth, B.E., Steere, A.N., Chasteen, N.D., Everse, S. J., Mason, A.B., (2011). How the binding of human transferrin primes the transferrin receptor potentiating iron release at endosomal pH. *Proc. Natl. Acad. Sci. U S A* **108**, 13089–13094.
3. Lawrence, C.M., Ray, S., Babyonyshev, M., Galluser, R., Borhani, D.W., Harrison, S.C., (1999). Crystal structure of the ectodomain of human transferrin receptor. *Science* **286**, 779–782.
4. Testi, C., Boffi, A., Montemiglio, L.C., (2019). Structural analysis of the transferrin receptor multifaceted ligand(s) interface. *Biophys. Chem.* **254**, 106242
5. Cheng, Y., Zak, O., Aisen, P., Harrison, S.C., Walz, T., (2004). Structure of the human transferrin receptor-transferrin complex. *Cell* **116**, 565–576.
6. Giannetti, A.M., Bjorkman, P.J., (2004). HFE and transferrin directly compete for transferrin receptor in solution and at the cell surface. *J. Biol. Chem.* **279**, 25866–25875.
7. West Jr., A.P., Giannetti, A.M., Herr, A.B., Bennett, M.J., Nangiana, J.S., Pierce, J.R., et al., (2001). Mutational analysis of the transferrin receptor reveals overlapping HFE and transferrin binding sites. *J. Mol. Biol.* **313**, 385–397.
8. Bennett, M.J., Lebron, J.A., Bjorkman, P.J., (2000). Crystal structure of the hereditary haemochromatosis protein HFE complexed with transferrin receptor. *Nature* **403**, 46–53.
9. Montemiglio, L.C., Testi, C., Ceci, P., Falvo, E., Pitea, M., Savino, C., et al., (2019). Cryo-EM structure of the human ferritin-transferrin receptor 1 complex. *Nat. Commun.* **10**, 1121.
10. Abraham, J., Corbett, K.D., Farzan, M., Choe, H., Harrison, S.C., (2010). Structural basis for receptor recognition by New World hemorrhagic fever arenaviruses. *Nat. Struct. Mol. Biol.* **17**, 438–444.
11. Radoshitzky, S.R., Abraham, J., Spiropoulou, C.F., Kuhn, J.H., Nguyen, D., Li, W., et al., (2007). Transferrin receptor 1 is a cellular receptor for New World haemorrhagic fever arenaviruses. *Nature* **446**, 92–96.
12. Gruszczyk, J., Kanjee, U., Chan, L.J., Menant, S., Malleret, B., Lim, N.T.Y., et al., (2018). Transferrin receptor 1 is a reticulocyte-specific receptor for Plasmodium vivax. *Science* **359**, 48–55.
13. Wang, X., Wen, Z., Cao, H., Luo, J., Shuai, L., Wang, C., et al., (2023). Transferrin receptor protein 1 is an entry factor for rabies virus. *J. Virol.* **97**, e0161222.
14. Fedeli, C., Moreno, H., Kunz, S., (2018). Novel insights into cell entry of emerging human pathogenic arenaviruses. *J. Mol. Biol.* **430**, 1839–1852.
15. Burri, D.J., da Palma, J.R., Kunz, S., Pasquato, A., (2012). Envelope glycoprotein of arenaviruses. *Viruses* **4**, 2162–2181.
16. Zeitlin, L., Geisbert, J.B., Deer, D.J., Fenton, K.A., Bohorov, O., Bohorova, N., et al., (2016). Monoclonal antibody therapy for Junin virus infection. *PNAS* **113**, 4458–4463.
17. Cohen-Dvashi, H., Amon, R., Agans, K.N., Cross, R.W., Borenstein-Katz, A., Mateo, M., et al., (2020). Rational design of universal immunotherapy for TfR1-tropic arenaviruses. *Nat. Commun.* **11**, 67.
18. Kariolis, M.S., Wells, R.C., Getz, J.A., Kwan, W., Mahon, C.S., Tong, R., et al., (2020). Brain delivery of therapeutic proteins using an Fc fragment blood-brain barrier transport vehicle in mice and monkeys. *Sci. Transl. Med.* **12**
19. Sjöström, D.J., Berger, S.A., Oberdorfer, G., Bjelic, S., (2020). Computational backbone design enables soluble engineering of transferrin receptor apical domain. *Proteins Struct. Funct. Bioinf.* **88**, 1569–1577.
20. Sjöström, D.J., Lundgren, A., Garforth, S.J., Bjelic, S., (2021). Tuning the binding interface between Machupo virus glycoprotein and human transferrin receptor. *Proteins Struct. Funct. Bioinf.* **89**, 311–321.
21. Sjöstrom, D.J., Mohlin, C., Ambrosetti, E., Garforth, S.J., Teixeira, A.I., Bjelic, S., (2022). Motif-driven protein binder design towards transferrin receptor helical domain. *FEBS J.* **289**, 2935–2947.
22. Singh, M.V., Weil, P.A., (2002). A method for plasmid purification directly from yeast. *Anal. Biochem.* **307**, 13–17.
23. Chao, G., Lau, W.L., Hackel, B.J., Sazinsky, S.L., Lippow, S.M., Wittrup, K.D., (2006). Isolating and engineering human antibodies using yeast surface display. *Nat. Protoc.* **1**, 755–768.
24. Benatuil, L., Perez, J.M., Belk, J., Hsieh, C.M., (2010). An improved yeast transformation method for the generation of very large human antibody libraries. *Protein Eng. Des. Sel.* **23**, 155–159.
25. Diederichs, K., Karplus, P.A., (1997). Improved R-factors for diffraction data analysis in macromolecular crystallography. *Nat. Struct. Biol.* **4**, 269–275.
26. Kabsch, W., (2010). Xds. *Acta Crystallogr. D Biol. Crystallogr.* **66**, 125–132.
27. McCoy, A.J., Grosse-Kunstleve, R.W., Adams, P.D., Winn, M.D., Storoni, L.C., Read, R.J., (2007). Phaser crystallographic software. *J. Appl. Cryst.* **40**, 658–674.

28. Adams, P.D., Afonine, P.V., Bunkoczi, G., Chen, V.B., Davis, I.W., Echols, N., et al., (2010). PHENIX: a comprehensive Python-based system for macromolecular structure solution. *Acta Crystallogr. D Biol. Crystallogr.* **66**, 213–221.
29. Shimon, A., Shani, O., Diskin, R., (2017). Structural basis for receptor selectivity by the whitewater arroyo mammarenavirus. *J. Mol. Biol.* **429**, 2825–2839.
30. Bridges, K.R., Smith, B.R., (1985). Discordance between transferrin receptor expression and susceptibility to lysis by natural killer cells. *J. Clin. Invest.* **76**, 913–918.
31. Radoshitzky, S.R., Longobardi, L.E., Kuhn, J.H., Retterer, C., Dong, L., Clester, J.C., et al., (2011). Machupo virus glycoprotein determinants for human transferrin receptor 1 binding and cell entry. *PLoS One* **6**, e21398.
32. Radoshitzky, S.R., Kuhn, J.H., Spiropoulou, C.F., Albarino, C.G., Nguyen, D.P., Salazar-Bravo, J., et al., (2008). Receptor determinants of zoonotic transmission of New World hemorrhagic fever arenaviruses. *Proc. Natl. Acad. Sci. U S A* **105**, 2664–2669.
33. Kerr, S.A., Jackson, E.L., Lungu, O.I., Meyer, A.G., Demogines, A., Ellington, A.D., et al., (2015). Computational and functional analysis of the virus-receptor interface reveals host range trade-offs in new world arenaviruses. *J. Virol.* **89**, 11643–11653.
34. Demogines, A., Abraham, J., Choe, H., Farzan, M., Sawyer, S.L., (2013). Dual host-virus arms races shape an essential housekeeping protein. *PLoS Biol.* **11**, e1001571.
35. Sahtoe, D.D., Coscia, A., Mustafaoglu, N., Miller, L.M., Olal, D., Vulovic, I., et al., (2021). Transferrin receptor targeting by de novo sheet extension. *Proc. Natl. Acad. Sci. U S A* **118**
36. Clark, L.E., Mahmutovic, S., Raymond, D.D., Dilanyan, T., Koma, T., Manning, J.T., et al., (2018). Vaccine-elicited receptor-binding site antibodies neutralize two New World hemorrhagic fever arenaviruses. *Nat. Commun.* **9**, 1884.
37. Otsuka, F.A.M., Bjelic, S., (2022). Evaluation of residue variability in a conformation-specific context and during evolutionary sequence reconstruction narrows drug resistance selection in Abl1 tyrosine kinase. *Protein Sci.* **31**, e4354.